Chemical Engineering Journal 162 (2010) 974–988

Contents lists available at ScienceDirect

Chemical Engineering Journal

journal homepage: www.elsevier.com/locate/cej

Modeling non-Fickian transport and hyperexponential deposition for deep bed filtration

Hao Yuan*, Alexander A. Shapiro

Department of Chemical and Biochemical Engineering, Technical University of Denmark, DTU, Building 229, 2800 Lyngby, Denmark

ARTICLE INFO

Article history:
Received 28 April 2010
Received in revised form 30 June 2010
Accepted 1 July 2010

Keywords:
Deep bed filtration
Temporal dispersion
Particle population heterogeneity
Hyperexponential deposition
Comparison with experiments

ABSTRACT

An integral model of the deep bed filtration process has been developed. It incorporates pore and particle size distributions, as well as the particle residence time distribution in the framework of the continuous time random walk theory. Numerical modeling is carried out to study the factors influencing breakthrough curves and deposition profiles for the deep bed filtration systems. Results are compared with a large set of experimental observations. Our findings show that highly dispersed breakthrough curves, e.g. those with early arrivals and large ending tails, correspond to large dispersion coefficients. For such cases the elliptic equation excels the advection dispersion equation in both fitting breakthrough curves and predicting deposition profiles related to natural or highly heterogeneous porous media. The deposition hyperexponentiality can be caused by the following three mechanisms: particle population in connection with the distribution of the filtration coefficients, heterogeneity in connection with non-Fickian transport, and heterogeneity in connection with the spatial distribution of the filtration coefficients. The influence and interaction of all three mechanisms have been analyzed in numerical computations and by comparison to several sets of experimental data.

1. Introduction

Modeling suspension or colloid flow in porous media is of great importance to a large variety of applications, e.g. deep bed filtration, membrane filtration, drilling mud filtration, bacteria and viruses spreading in underground water and others [1,2]. There is a considerable and ongoing effort aimed at understanding the transport and the deposition of suspended particles in porous media. Especially, non-Fickian transport and non-exponential deposition of particles, such as hyperexponential and non-monotonic deposition profiles, attract significant interest [3–7].

The physical heterogeneity of porous media leads to non-Fickian behavior of the suspensions in porous media [3–6]. Recent works indicate that non-Fickian transport of a solute or a suspension may be modeled more accurately by approaches based on the continuous time random walk (CTRW) theory compared to the classical advection dispersion equation (ADE) [4,5]. In the framework of the CTRW approach A. Shapiro and P. Bedrikovetsky proposed a macroscopic elliptic equation for non-Fickian transport in porous media [6,7]. Recently, the approach has been extended in order to incorporate the distributed particles, as well as plugging of the porous medium [8]. Compared to the conventional ADE the elliptic equation has two additional terms reflecting the distributed residence time or flight time of the particles: the temporal dispersion term and the mixed dispersion term. In cases where the particles of n different types are filtered in a porous medium, n elliptic equations (plus deposition-plugging equations) are required for description of the filtration. Continuous distributions of the particles are approximated by discrete distributions with several particle types, as described below.

The conventional methodology, ADE with a single filtration coefficient, merely predicts exponentially decreasing deposition profiles [9,10]. Many of the experimental results, on the other hand, show hyperexponential deposition profiles or even non-monotonic deposition profiles under some specific conditions [1,10–12].

It is believed that the heterogeneity of the particle population or the heterogeneity of particle-medium-interaction is the main reason for hyperexponential deposition profiles in homogeneous porous media [10,13]. The heterogeneity of the particle population encompasses the physical heterogeneity (size and shape) and the physiochemical heterogeneity (surface charge and multiple energy minima). For instance, in a deep bed filtration system which the size exclusion mechanism dominates, the larger particles deposits faster and correspond to larger filtration coefficients. The distribution of filtration coefficients is most likely dependent on the particle size distribution [8]. Even flow of a monodisperse suspension (uniform shape and size) in a homogeneous porous medium under unfavorable attachment conditions is observed to result

* Corresponding author. Tel.: +45 45252864.
E-mail address: hy@kt.dtu.dk (H. Yuan).

1385-8947/$ – see front matter © 2010 Elsevier B.V. All rights reserved.
doi:10.1016/j.cej.2010.07.003

Nomenclature

c_i	Number of suspended particles per unit pore volume (m^{-3})
C_i	Dimensionless suspended particle concentration
s_i	Number of retained particles per unit volume of porous media
S_i	Dimensionless retained particle concentration
t	Time (s)
T	Dimensionless time (pore volume)
x	x coordinate in space
X	Dimensionless x
N_c	Number of retained particles per gram of porous media
N_t	Number of total injected particles
v	Interstitial velocity of particles
u	Dimensionless interstitial velocity of particles
D_x	Coefficient of spatial dispersion (m^2/s)
D_t	Coefficient of temporal dispersion (s)
R_x	Dimensionless longitudinal dispersivity
R_t	Dimensionless temporal dispersivity
p	Probability density function
a	Coefficient in power law distribution
b	Power in the power law distribution
f_{low}	Fraction of the component with low Λ in the bimodal distribution
f_{high}	Fraction of the component with high Λ in the bimodal distribution
t_0	Particle injection duration (s)
T_0	Particle injection duration (pore volume)
c_0	Influent concentration
μ	Mean value
σ	Standard deviation
λ	Filtration coefficient (s^{-1})
Λ	Dimensionless filtration coefficient
ξ	Total injection time is ξ times the particle injection duration
φ	Porosity of the porous media
ρ_b	Bulk density of the dry porous media

sometimes in a hyperexponential deposition profile, due to the heterogeneity of particle surface charge and second energy minimum [10,14]. Mathematically, the heterogeneity of the particle population is described by the distribution of the filtration coefficients. The deposition patterns may be interpreted by application of various distribution types: the log-normal distribution, the power law distribution, the bimodal distribution and others [14,15].

In order to study how the heterogeneity of the particle population leads to hyperexponential deposition profiles, it is important to separate its influence from the effect of heterogeneity of porous media. Lots of the relevant studies focus on the physically homogeneous porous media, e.g. packed glass beads in the column [16–18]. Some experiments have been carried out in micro-heterogeneous porous media, e.g. packs of natural quartz sand [19–21]. Other experiments adopt specially constructed porous media with heterogeneity on a mesoscale [5,22]. The data from pilot experiments of mainly tracers in natural/highly heterogeneous porous media and porous rocks is also available [23].

In this paper, the factors controlling the deposition profiles and the shape of breakthrough curves are systematically studied. An integral model is applied. It incorporates both the distribution of the filtration coefficients (as in Refs. [15,24]) and the distributed particle flight time (as in Refs. [6–8]). A large set of data obtained in the experiments with homogeneous and heterogeneous porous media is compared with the results from the numerical modeling. Apart from the data on deep bed filtration experiments, data on tracer injection have been used, since tracers may be considered as "suspensions with a zero-filtration coefficient". The goal of the comparison is to find out which mechanisms incorporated in the model are necessary in order to reproduce the experimental results successfully: either temporal dispersion of particle flights or distribution of filtration coefficients, or both of them.

The paper is organized as follows. Section 2 introduces the integral model incorporating the elliptic equation in connection with non-Fickian transport in heterogeneous porous media and the distributed filtration coefficients in connection with particle population heterogeneity. Section 3 presents the results of the numerical modeling, to study how various factors influence the breakthrough curves and the deposition profiles. Section 4 describes a comparison of the results from different models to the experiments carried out with the different porous media, to study which model is proper under which experimental conditions. Finally, the conclusions are drawn.

2. Modeling

2.1. Elliptic equation

It has been suggested in Refs. [6–8] that transport of a dilute monodisperse suspension in a porous medium may be described by an elliptic equation accounting for particle advection, spatial dispersion, temporal dispersion, mixed dispersion, and deposition. The temporal dispersion represents the effects of the distributed residence time of the particles in various pores. This is a simple way to formalize the Continuous Time Random Walk (CTRW) approach, where dispersion of a time step is usually expressed by means of a distribution kernel [4,5]. It has been shown [6,7] that in the limit of infinitely many infinitely small time steps and a finite variance of a single step, the distribution may be represented by the two coefficients D_t, D_{xt} (for temporal and mixed dispersion), and instead of the convolution with the distribution kernel, it is enough to consider the terms with the second time derivative and with the mixed derivative, making the transport equation elliptic.

In this work we study the application of the elliptic formalism to filtration of the diluted suspensions of particles, which are normally applied in the experiments. Since the suspended concentrations in the reported experiments are fairly low to influence the pore structure, this influence is neglected. The mixed dispersion is also neglected, since it has no qualitative influence on the profiles. In order to reveal the heterogeneity of the particle population the particles are split into portions, i.e. there are multiple equations representing different particle species with various filtration coefficients. Under these conditions, the suspended concentration $c_i(x,t)$ and the deposited concentration $s_i(x,t)$ of the ith component of the suspension at column depth x and time t are modeled by the elliptic equation with a sink term representing the deposition of the particles:

$$\frac{\partial c_i}{\partial t} + v_i \frac{\partial c_i}{\partial x} = D_x \frac{\partial^2 c_i}{\partial x^2} + D_t \frac{\partial^2 c_i}{\partial t^2} - \lambda_i c_i \tag{1}$$

After this equation has been solved the deposition of the particles of the ith type may be found by integrating

$$\frac{\partial s_i}{\partial t} = \lambda_i c_i \varphi \tag{2}$$

Summation of s_i gives the total deposition at a given time.

In Eqs. (1) and (2), v_i is the interstitial particle velocity, D_x is the spatial dispersion coefficient, D_t is the temporal dispersion coefficient, which by definition is the second moment of the particle residence time divided by the first moment of the particle residence

time to zero, λ_i is the filtration coefficient of the ith species of the particles, and φ is the bed porosity. The suspended concentration has the dimension of the number of particles per pore volume and the retention concentration of the number of particles per unit volume of the porous medium. For convenience of comparison to the experiments, the following practical quantities are often adopted: N_c is the number of the retained particles per gram of dry porous media, and N_t the total number of injected particles [10,19,25].

$$N_c = \sum_{i=1,2,3,\ldots}^{N} \frac{s_i}{\rho_b};$$
$$N_t = c_0 t_0 v;$$

where ρ_b is the bulk density of the dry porous media, t_0 is the particle injection duration, and c_0 is the influent concentration. In dimensionless coordinates the elliptic equation for the ith particle species takes the form [8]:

$$\frac{\partial C_i}{\partial T} + u\frac{\partial C_i}{\partial X} = uR_{xi}\frac{\partial^2 C_i}{\partial X^2} + \frac{R_{ti}}{u}\frac{\partial^2 C_i}{\partial T^2} - \Lambda_i C_i \tag{3}$$

$$\frac{\partial S_i}{\partial t} = \Lambda_i C_i \varphi \tag{4}$$

where the following substitutions are introduced to the system:

$$x = LX; \qquad t = \left(\frac{L}{v_0}\right)T; \qquad c_i = C_i c_0; \qquad s_i = S_i c_0; \qquad v = uv_0;$$

$$R_{xi} = \frac{D_{xi}}{v_0 L}; \qquad R_{ti} = \frac{D_{ti}v_0}{L}; \qquad \Lambda_i = \frac{\lambda_i L}{v_0};$$

Here R_{xi} is the dimensionless longitudinal dispersivity and R_{ti} is the dimensionless temporal dispersivity of the ith component. The value of L is the reference length (m), v_0 is the reference velocity (m/s), and c_0 is the reference concentration. The inverse Peclet number R_{xi} describes the magnitude of the spatial dispersion compared to the product of the reference velocity and the reference length, while the similar parameter R_{ti} describes the magnitude of the temporal dispersion compared to the reference time.

2.2. Distributed filtration coefficients

The log-normal distribution, the power law distribution and the bimodal distribution are commonly adopted to reflect the particle population heterogeneity [15,24,26–28]. The probability density function (PDF) for the log-normal distributed filtration coefficients is of the following form:

$$p(\Lambda_i) = \frac{1}{\Lambda_i \sigma\sqrt{2\pi}}\exp\left[\frac{(\ln\Lambda_i - \mu)^2}{2\sigma^2}\right] \tag{5}$$

where μ and σ are the mean and the standard deviation of the natural logarithm of the filtration coefficients. The power law distribution takes the form:

$$p(\Lambda_i) = a(\Lambda_i)^{-b}, \qquad \Lambda_i \in [\Lambda_{\min}, \Lambda_{\max}] \tag{6}$$

where a and b are two positive constants controlling the shape of the distribution. The larger b the more asymmetric PDF curve. Constant a is selected so that the sum of the probabilities of appearance of the different values of Λ is equal to unity (the value of $\Delta\Lambda = \Lambda_i - \Lambda_{i-1}$ is selected to be constant):

$$a = \frac{1}{\sum_{i=1,2,\ldots}^{N}(\Lambda_i)^{-b}} \tag{7}$$

The limitation $[\Lambda_{\min}, \Lambda_{\max}]$ is necessary, since otherwise the integral of the distribution is divergent on $[0,\infty]$. In accordance with previous works, the distribution is selected so that the integral is divergent at infinity, and so that dependence on the upper limit of integration becomes important.

Discrete binary filtration coefficients reflecting heterogeneity of a particle population are proposed in several studies [26–28]. This type of distribution is adopted to model the following case scenarios. Under unfavorable surface conditions, the colloid deposition can be classified into two categories: the unhindered particle deposition into a relatively deep secondary energy well (fast) and the particle deposition overcoming an energy barrier to reach the primary energy minimum [10,14]. Here a bimodal distribution consisting of two normal subdistributions is adopted and takes the following form:

$$p(\Lambda_i) = f_{low}\frac{1}{\sigma_{low}\sqrt{2\pi}}\exp\left[-\frac{1}{2}\left(\frac{\Lambda_i - \Lambda_{low}}{\sigma_{low}}\right)^2\right] + f_{high}\frac{1}{\sigma_{high}\sqrt{2\pi}}\exp\left[-\frac{1}{2}\left(\frac{\Lambda_i - \Lambda_{high}}{\sigma_{high}}\right)^2\right] \tag{8}$$

where Λ_{low} and Λ_{high} are the mean filtration coefficients of the two normal subdistributions,σ_{low} and σ_{low} are the corresponding standard deviations, and f_{low} and f_{high} are the fractions of the total population associated with each subdistribution.

In the following computations, it is assumed that the interstitial velocities of the particles of various sizes are the same. They may either be approximated by the average pore velocity, or need to be fitted to the experimental results. On the contrary, the filtration coefficients may be different. To approximate the continuous distribution of them, the particle population is simply discretized into 1000 representative species, each of which is assigned a single filtration coefficient. The proportion of each species is calculated in accordance with the continuous expression. However, the sum of the proportions is not unity, due to a local truncation error and a truncation of Λ close to infinity. It is then normalized by dividing the sum by itself. The procedure needs two artificial values: the minimum and the maximum of the filtration coefficients. This is especially related to the power distribution, as discussed above.

2.3. Boundary conditions

The adopted boundary conditions here are ad hoc for the system of elliptic equations. There are four boundary conditions in the space-time plane: the initial condition (9), the terminal condition (10), the inlet condition (11), (12), and the outlet condition (13):

$$C_i(X, 0) = 0 \tag{9}$$

$$C_i(X, \xi T_0) = 0 \tag{10}$$

$$C_i(0, T) = 1, \quad 0 < T < T_0 \tag{11}$$

$$C_i(0, T) = 0, \quad T_0 \le T \le \xi T_0 \tag{12}$$

$$\left.\frac{dC_i}{dX}\right|_{X=1} = 0 \tag{13}$$

This is rather different from the boundary conditions for the parabolic ADE, in that the second derivative in the temporal dispersion term here requires an additional temporal boundary condition. The details are discussed in Ref. [8].

The four boundary conditions are selected to model column experiments in most labs. Before the injection the column is often flooded with pure water to make the bed clean. Thus, condition (9) reflects absence of suspended particles in the bed prior to flooding. The influent concentration is set to be constant during the particle injection time T_0 (boundary condition (10)). Pure water is injected after the suspension injection, so that all the suspended particles are flushed out of the system (boundary condition (12)). The value

ξ is selected so that after ξT_0 the suspended concentration is effectively zero, hence, the final condition (10). Our computations show that any value of $\xi \geq 5$ provides the same shape of solutions.

2.4. Degree of hyperexponentiality

In order to quantitatively describe the degree of hyperexponentiality in the deposition profiles, the following definitions are introduced. Providing that the dimensionless retained particle concentration is a function in terms of dimensionless X, $S(X)$ and the deposition is monotonically decaying with X, $S'(X) \leq 0$, the degree of the hyperexponentiality is

$$DH = \frac{\max[d(\ln S)/dX] - \min[d(\ln S)/dX]}{\max[d(\ln S)/dX]} \quad (14)$$

The values of DH are listed in the tables reflecting the results of the computations.

2.5. Implementation

Direct discretization of Eqs. (3) and (4) by a finite difference method results in a system of linear algebraic equations for each point on a rectangular grid. A center difference regime is adopted to achieve accuracy of second order, $O(\Delta X^2)$ and $O(\Delta T^2)$. The computation is implemented in MATLAB, utilizing its fast implementation of the matrix operations [29]. To achieve higher accuracy the mesh grid is set to be 1000×1000. In the calculations sparse matrices are adopted for the purpose of memory optimization and fast computation [30]. In order to demonstrate the reliability of the program, a calculation is performed with the same configurations as those in Refs. [7,15]. Especially, D_t is set to be zero and for the distribution the number of particle species is 1000 to achieve high accuracy. The numerical solution highly agrees with the analytical solution for the unsteady state in Ref. [15], with an average difference of 0.1%. In order to fit the experimental breakthrough curves, the dispersion coefficients and the filtration coefficients are modified manually. Predicted deposition profiles can then be compared to the experimental observations. Especially for the distributed filtration coefficients further adjustments are needed to fit the hyperexponential deposition profiles.

3. Results of numerical modeling

The goal of this section is to find out which parameters have most influence on the shapes of the deposition profiles and breakthrough curves. First, a number of computations have been performed with the ADE and the different distributions for Λ. Next, the results of the elliptic modeling have been obtained and the effects of the temporal dispersion on the breakthrough curves and deposition profiles have been studied. Finally, the combined influences of both the temporal dispersion and the distribution of Λ have been studied.

3.1. ADE with distributed Λ

Calculations are first performed without the temporal dispersion but only with the distributed filtration coefficients. The log-normal distribution, the power law distribution and the bimodal distribution are the adopted three types of distributions.

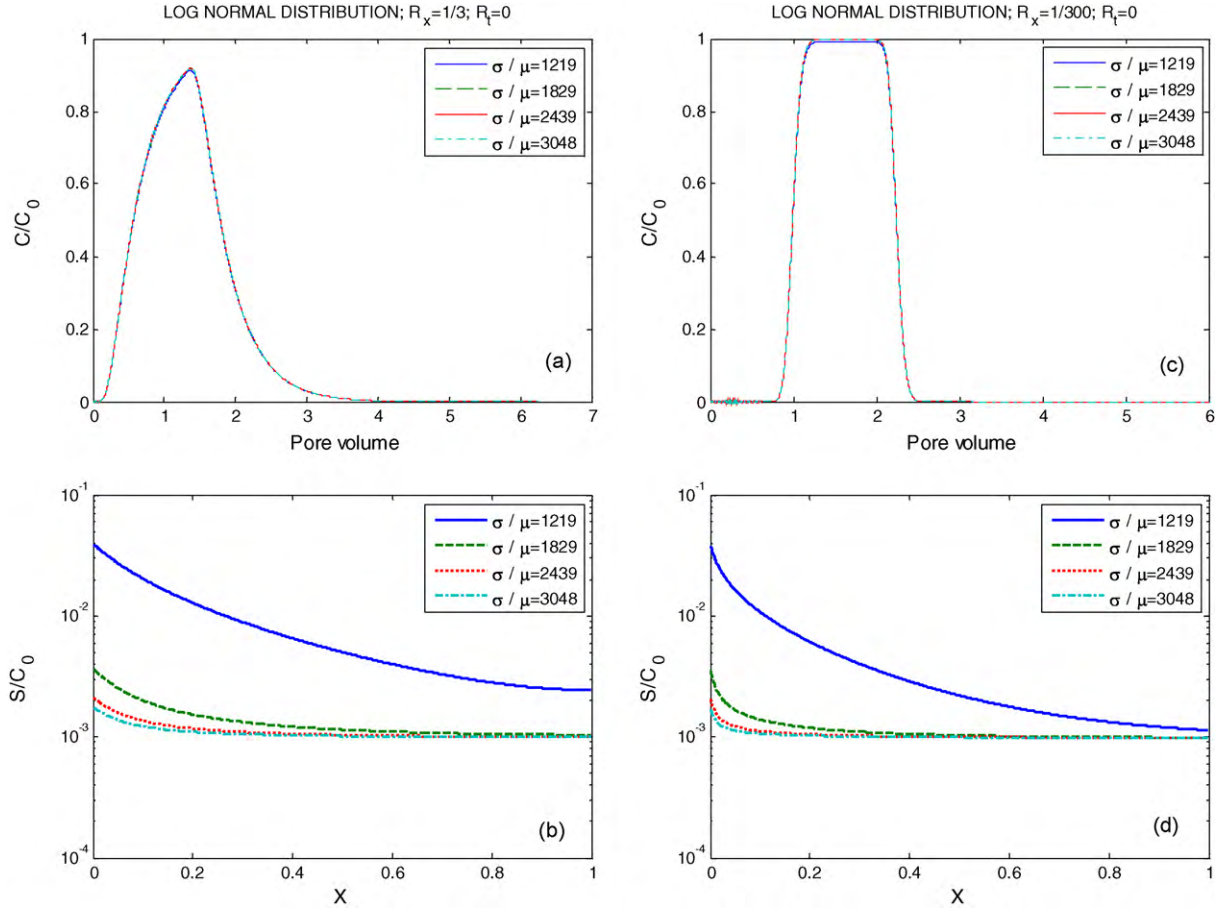

Fig. 1. Breakthrough curves and deposition profiles with log-normal distribution of filtration coefficients, (a) and (b): large spatial dispersion; (c) and (d): small spatial dispersion.

Table 1
Parameters adopted for calculations with the log-normal distribution of filtration coefficients and resulting degrees of hyperexponentiality. Results are shown in Fig. 1.

σ/μ	σ ($\times 10^3$)	R_x	DH
1219	2.4	$3^{-1}/30^{-1}$	69.03/45.41
2032	4.0	$3^{-1}/30^{-1}$	193.23/724.23
2845	5.6	$3^{-1}/30^{-1}$	362.54/1076.01
3658	7.2	$3^{-1}/30^{-1}$	488.91/1088.23

Table 2
Parameters adopted for calculations with the power law distribution of filtration coefficients and resulting degrees of hyperexponentiality. Results are shown in Fig. 2.

$\sigma/\Lambda_{\min}$	σ ($\times 10^3$)	R_x	b	DH
26,754	574,821	$3^{-1}/300^{-1}$	0.80	136,320/200,920
1871	3682	$3^{-1}/300^{-1}$	1.20	26,824/1420
133	263	$3^{-1}/300^{-1}$	1.60	19,969/28.35
9	20	$3^{-1}/300^{-1}$	2.00	1.03/1.08

Results under the condition of both large and small spatial dispersion are compared for the calculations with the log-normal distribution and the power law distribution.

For the log-normal distribution the mean value of the filtration coefficients is kept constant, while the standard deviations vary. Other invariable parameters are: $\mu = 1.97$, $T_0 = 1.25PV$, $u = 1$, $R_t = 0$, $R_x = 1/30$, $\Lambda_{\min} = 2 \times 10^{-3}$, $\Lambda_{\max} = 394$. The rest of the parameters adopted in the calculations are shown in Table 1. As seen in Fig. 1, the results show that the log-normal distribution of Λ gives rise to hyperexponential deposition profiles, but only has a minor influence on the breakthrough curves. The degree of hyperexponentiality is limited. Even extremely large standard deviations do not produce extremely hyperexponential profiles.

For the power law distribution, different values of power b (see Eq. (6)) are chosen to vary the distribution. The maximum and the minimum of the distribution are kept constant. For different calculations: $T_0 = 1.25PV$, $u = 1$, $R_t = 0$, $R_x = 1/30$, $\Lambda_{\min} = 2 \times 10^{-3}$, $\Lambda_{\max} = 1968$. The rest of the parameters adopted for the calculations are shown in Table 2. As seen in Fig. 2, the results are similar to the log-normal distribution: the power law distribution of Λ results in hyperexponential deposition profiles, but only has a minor influence on the breakthrough curves. The distributions with the larger standard deviations yield higher hyperexponentiality. A larger standard deviation reflects a higher heterogeneity of the particle population. This confirms that one of the reasons for hyperexponential deposition profiles may be heterogeneity of the particle population [10,24]. The degree of hyperexponentiality with the power law distribution of Λ is generally higher than with the log-normal distribution of Λ.

Calculations with the different maxima and minima of the power distribution $\Lambda_{\min}$, $\Lambda_{\max}$ have also been carried out. Results (not given here) show that the minimum of the distribution does not affect much the degree of hyperexponentiality, but still may slightly change the shape of a deposition profile. Increasing the maximum of the distribution mainly increases the retained concentration close to the inlet; therefore the degree of the hyperexponentiality also increases.

For the bimodal distribution, the fractions and the standard deviations of the two groups are set to be equal at first. For different calculations: $T_0 = 1.25PV$, $u = 1$, $R_t = 0$, $R_x = 1/30$, $\Lambda_{\min} = 2 \times 10^{-3}$,

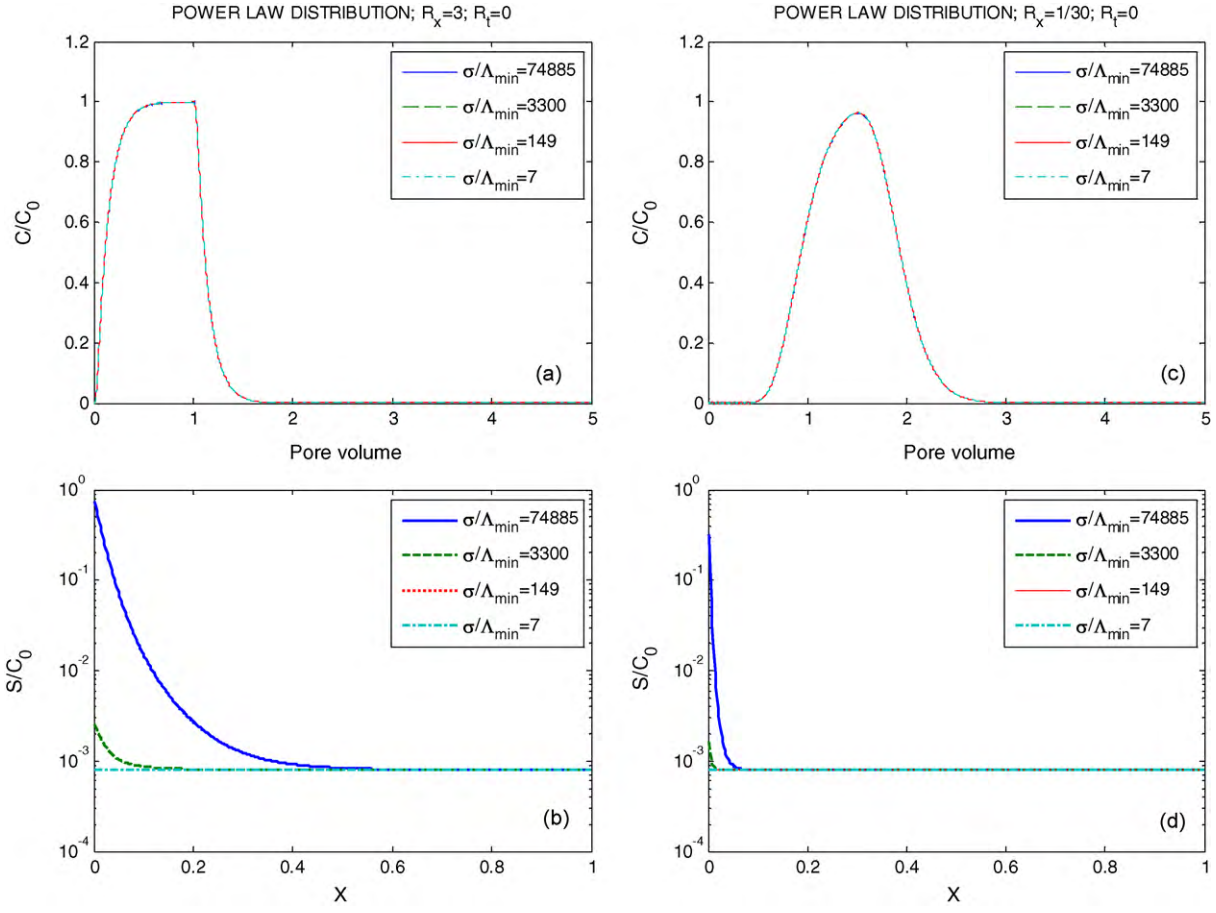

Fig. 2. Breakthrough curves and deposition profiles with power law distribution of filtration coefficients, (a) and (b): large spatial dispersion; (c) and (d): small spatial dispersion.

Table 3
Parameters adopted for calculations with bimodal distribution of filtration coefficients and resulting degrees of hyperexponentiality. Results are shown in (a) and (b) of Fig. 3.

$\Lambda_{high}/\Lambda_{low}$	Λ_{high}	Λ_{low}	DH
1.00	1.20	1.20	0
67.33	80.80	1.20	35.35
133.67	164.40	1.20	54.71
200.00	240.00	1.20	69.36

Table 4
Parameters adopted for calculations with bimodal distribution of filtration coefficients and resulting degrees of hyperexponentiality. Results are shown in (c) and (d) of Fig. 3.

f_{high}/f_{low}	f_{high}	f_{low}	DH
0	0	1.00	0
1/3	0.25	0.75	13.92
1	0.50	0.50	14.69
3	0.75	0.25	14.94
Inf	1.00	0	0

$\Lambda_{\max} = 1968$, $\sigma_{high} = 1.2$, $\sigma_{low} = 1.2$, $f_{high} = 0.5$. The rest of the parameters are shown in Table 3. First, Λ_{low} is kept constant and various Λ_{high} is selected. The influence of the difference between Λ_{high} and Λ_{low} is seen in Fig. 3(a) and (b). The profile may be split roughly into two almost "exponential" parts, with the different inclinations of the decay. With increasing difference between Λ_{high} and Λ_{low}, the deposition profile becomes more hyperexponential.

Then Λ_{high} and Λ_{low} are kept constant, and various fractions of the two species are selected. The selected parameters for the calculations are: $\Lambda_{high} = 24$, $\Lambda_{low} = 1.2$, $T_0 = 1.25PV$, $u = 1$, $R_t = 0$, $R_x = 1/30$, $\Lambda_{\min} = 2 \times 10^{-3}$, $\Lambda_{\max} = 1968$, $\sigma_{high} = 1.2$, $\sigma_{low} = 1.2$ and the rest of the parameters are given in Table 4. When the fractions of the different particles vary from $f_{high} = 0$, $f_{low} = 1$ to $f_{high} = 1$, $f_{low} = 0$, i.e. from the single component with low Λ to the single component with high Λ, the deposition decay changes from exponentiality to hyperexponentiality, and then to exponentiality again, as seen in Fig. 3(d). Thus, hyperexponentiality is observed in the systems with significant amounts of particles of different sizes, as in Refs. [10,24].

As seen in Fig. 3(d), the part of the deposition profile close to the inlet is formed by the particles with high Λ. The rest of the profile by the particles with low Λ. The regions of dominance of the two species depend on the ratio f_{high}/f_{low}. For high values of f_{high}/f_{low} the particles with high values of Λ remain close to the inlet, while the particles with low Λ travel further, close to the outlet. The resulting deposition profiles look like a combination of the two straight-linear intervals, respectively, corresponding to the high and the low values of Λ.

Unlike the log-normal distribution and the power law distribution, the bimodal distribution of filtration coefficients highly influences the breakthrough curves, as seen in Fig. 3(a).

In summary of the above results, the distribution of Λ can give rise to highly hyperexponential deposition profiles if the standard deviations are very large. Similar phenomena have been observed in Refs. [15,24]. Such a wide distribution of filtration coefficients may be doubted for the systems of similar particles. Therefore, the

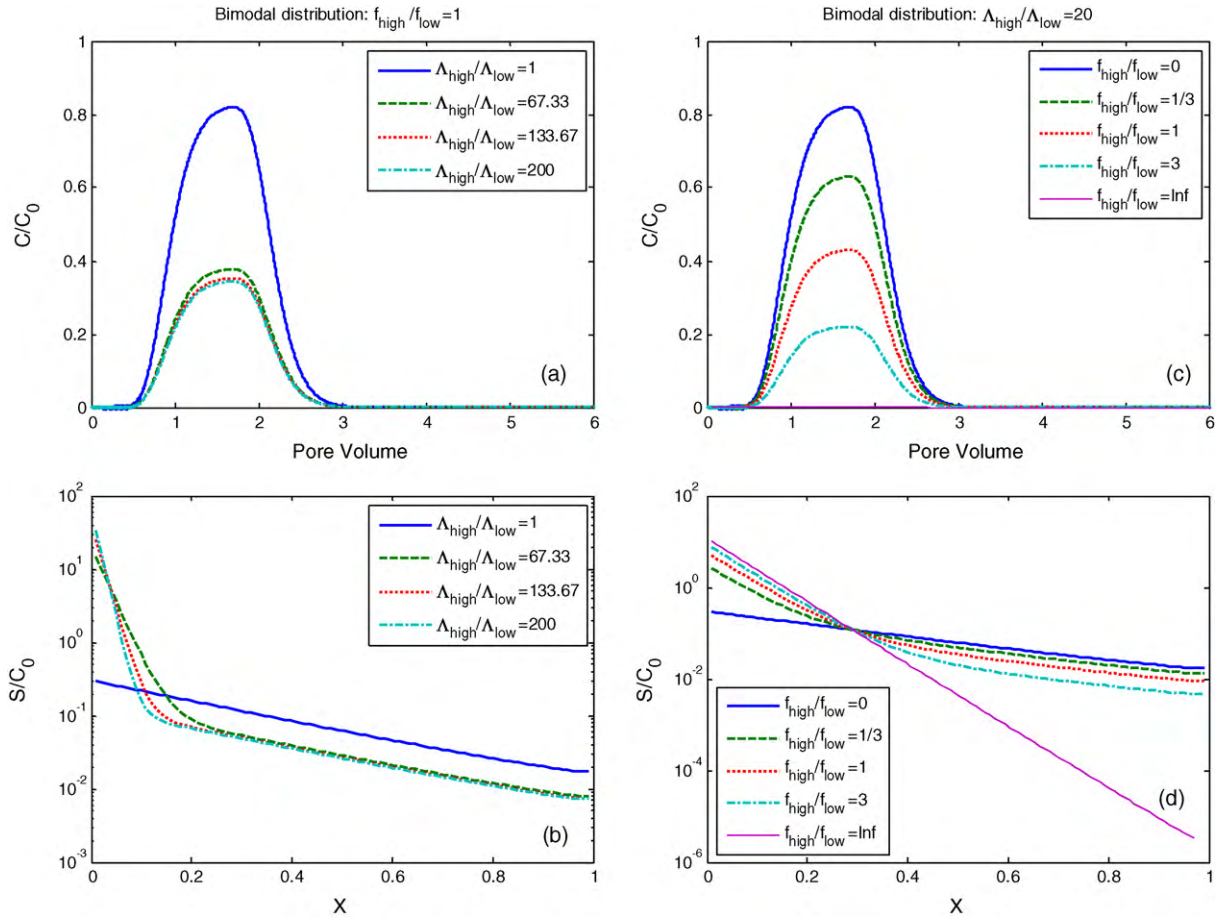

Fig. 3. Breakthrough curves and deposition profiles with bimodal distribution of filtration coefficients. (a) and (b) Keeping the fractions, standard deviations and Λ_{low}, change of Λ_{high}. (c) and (d) Keeping Λ_{low}, Λ_{high} and the standard deviations, change of f_{low}, f_{high}.

Table 5
Parameters adopted for calculations with elliptic equation and a single filtration coefficient and resulting degrees of hyperexponentiality. Results are shown in Fig. 4.

R_x	R_t	DH
$3/300^{-1}$	0	0/0
$3/300^{-1}$	22.00	155.56/6.17
$3/300^{-1}$	44.00	153.27/6.95
$3/300^{-1}$	66.00	154.39/6.71

Table 6
Parameters adopted for illustration of the distribution of filtration coefficients, compensated for by temporal dispersion. Results are shown in Fig. 5.

$\sigma/\Lambda_{\min}$	R_t	b
171	8.9286	1.1
93	8.9286	1.3
14	8.9286	10
171	4.4643	1.1
93	9.8214	1.3
14	11.1607	10

question arises, whether the temporal dispersion, in combination with somehow narrower distributions of the filtration coefficients (or, even, with a single filtration coefficient), may also result in a hyperexponential deposition profile.

3.2. Elliptic equation with a single Λ

Let us now present the results with $D_t > 0$. The calculations are performed for a suspension characterized by a single filtration coefficient. The values used for the calculations are $T_0 = 5PV$, $u = 1$, $\Lambda = 0.49$ and the rest of the values are shown in Table 5. The effects of the temporal dispersion both on the breakthrough curves and the deposition profiles are illustrated in Fig. 4.

As seen from the figure, temporal dispersion not only leads to hyperexponentiality of the deposition but also has a clear influence on the breakthrough curves. The delayed peaks and large ending tails are characteristic of the elliptic dispersivity. Similar effects have been observed in nature and in the experiments with stochastically heterogeneous porous media [4–8,31]. The degree of hyperexponentiality caused by temporal dispersion, on the other hand, is relatively limited.

The temporal dispersion works in combination with the spatial distribution. As seen in Fig. 4(a) and (c), large spatial dispersion may partly compensate for some influence of the temporal dispersion on the breakthrough curve. This unusual phenomenon is opposite to the effect of the spatial dispersion in absence of the temporal dispersion. On the other hand, it enhances the hyperexponentiality caused by the temporal dispersion in the deposition profiles.

3.3. Elliptic equation with distributed Λ

As seen from the results above, both the temporal dispersion and the distribution of the filtration coefficients give rise to the deposition hyperexponentiality. This section focuses on how the two factors in combination affect the breakthrough curves and the deposition profiles, and whether their effects can be complemented or compensated for by each other.

As an example, a system with power law distributed filtration coefficients has been studied. In the calculations: $T_0 = 2.17PV$, $u = 1$, $R_x = 1.79$, $\Lambda_{\min} = 0.896$, $\Lambda_{\max} = 1344$, and the rest of the parameters are shown in Table 6. In the first series of computations, power b

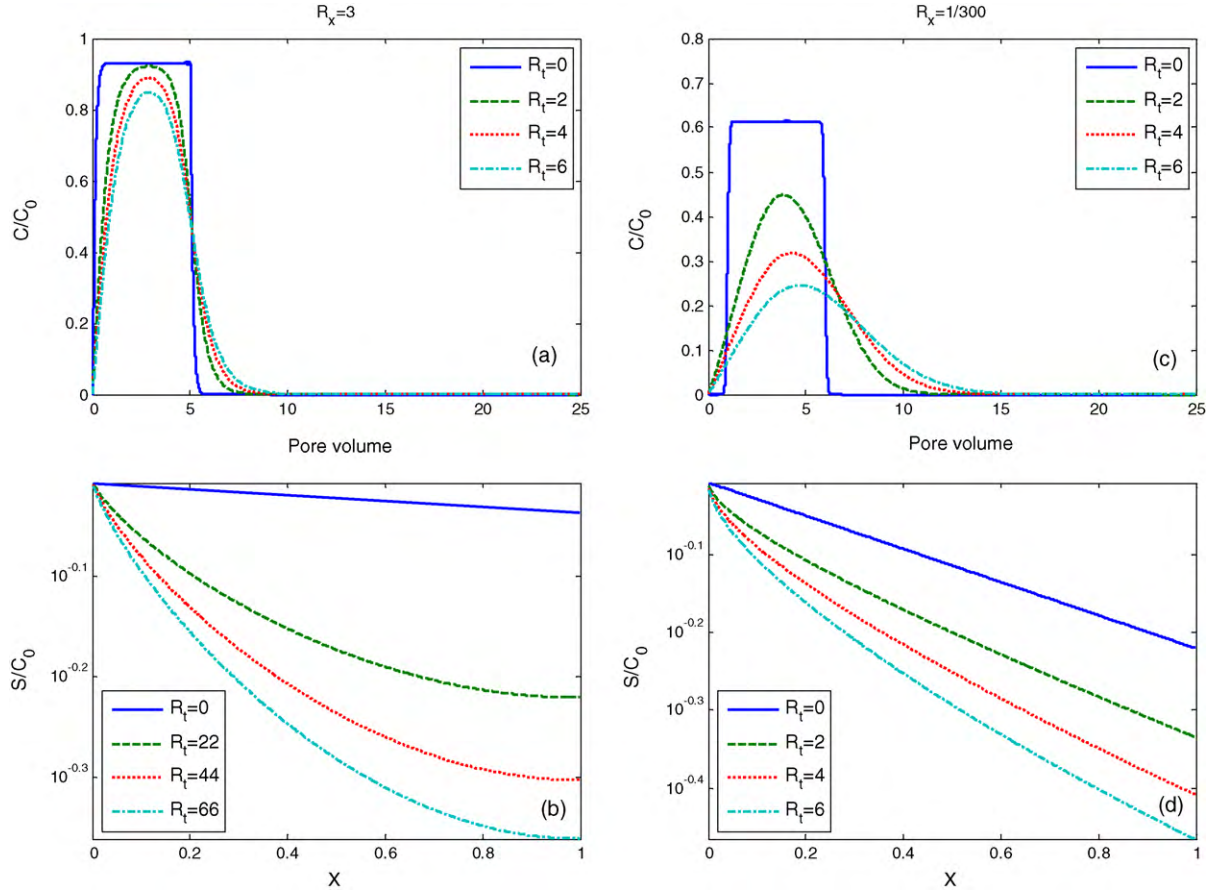

Fig. 4. Breakthrough curves and deposition profiles with a single filtration coefficient, (a) and (b): large spatial dispersion; (c) and (d): small spatial dispersion.

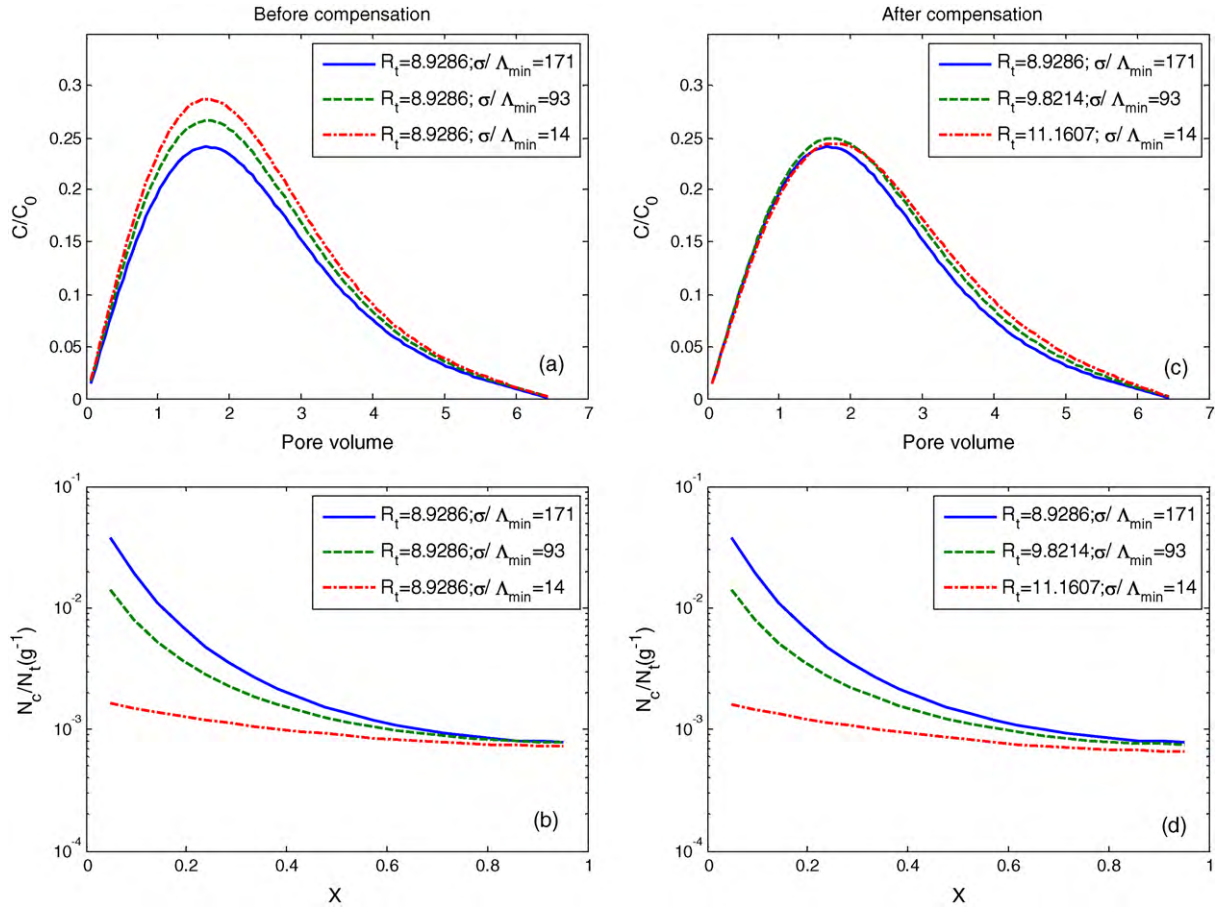

Fig. 5. Illustration of the distribution of filtration coefficients compensated for by the temporal dispersion. (a) and (b) Decrease of the standard deviation of the distribution with constant temporal dispersion. (c) and (d) Decrease of the standard deviation of the distribution with increasing temporal dispersion.

in the distribution is increased to reduce the standard deviation, and the minimum and maximum of the filtration coefficients are kept constant. It causes the deviations both in the breakthrough curves and the deposition profile, as seen in Fig. 5(a) and (b). Then the temporal dispersion is increased to compensate for loss of the distribution width. The breakthrough curves are recovered, but the deposition profiles still deviate, as seen in Fig. 5(c) and (d). Thus, the influence of the distribution of Λ on the breakthrough curves can be well compensated for by temporal dispersion, but that on the deposition profiles cannot.

A possibility of opposite compensation was also checked. Under the above conditions, the parameters are modified according to Table 7. With increased temporal dispersion and invariable distribution of Λ, the deviation in the deposition profile, was minor but the BTC deviated significantly, as seen in Fig. 6(a) and (b). Then the standard deviation of the distribution is decreased to compensate for the increased temporal dispersion. The BTC was recovered, but the deposition profiles still deviated (Fig. 6(c) and (d)). This indicates that the influence of the temporal dispersion can be compensated for by the distribution of the filtration coefficients to some extent, but not entirely.

Selection of more flexible distributions and fitting multiple parameters might, of course, lead to complete compensation for the effect of temporal dispersion. However, these calculations show that, at least, the three distributions considered above provide breakthrough curves and deposition profiles possessing individual features, which may be different from the features of the profiles produced by non-zero temporal dispersion. They are clearly distinguishable, and interaction between them may contribute to better reproduction of the results. Especially breakthrough curves are affected. The cases of clearly dispersed breakthrough curves require introduction of temporal dispersion for fitting, while the cases where the breakthrough curves are not dispersed, but the deposition profiles are hyperexponential, require fitting with the distributed filtration coefficients alone.

4. Comparison with experiments

In this section the results of various modeling methodologies are compared to the experiments carried out with the different porous media reported in the literature. The purpose is to find out which modeling methodology is proper under which experimental conditions. The porous media range from the most homogeneous porous media, e.g. packed glass beads, to the most heterogeneous porous media, e.g. natural aquifer material. Since tracers may be considered as suspensions not exhibiting deposition, the experiments with them are also considered.

Table 7
Parameters adopted for illustration of temporal dispersion, compensated for by the distribution of filtration coefficients. Results are shown in Fig. 6.

$\sigma/\Lambda_{\min}$	R_t	b
291	4.4643	0.89
291	6.6964	0.89
291	8.9286	0.89
291	4.4643	0.89
171	6.6964	1.1
43	8.9286	10

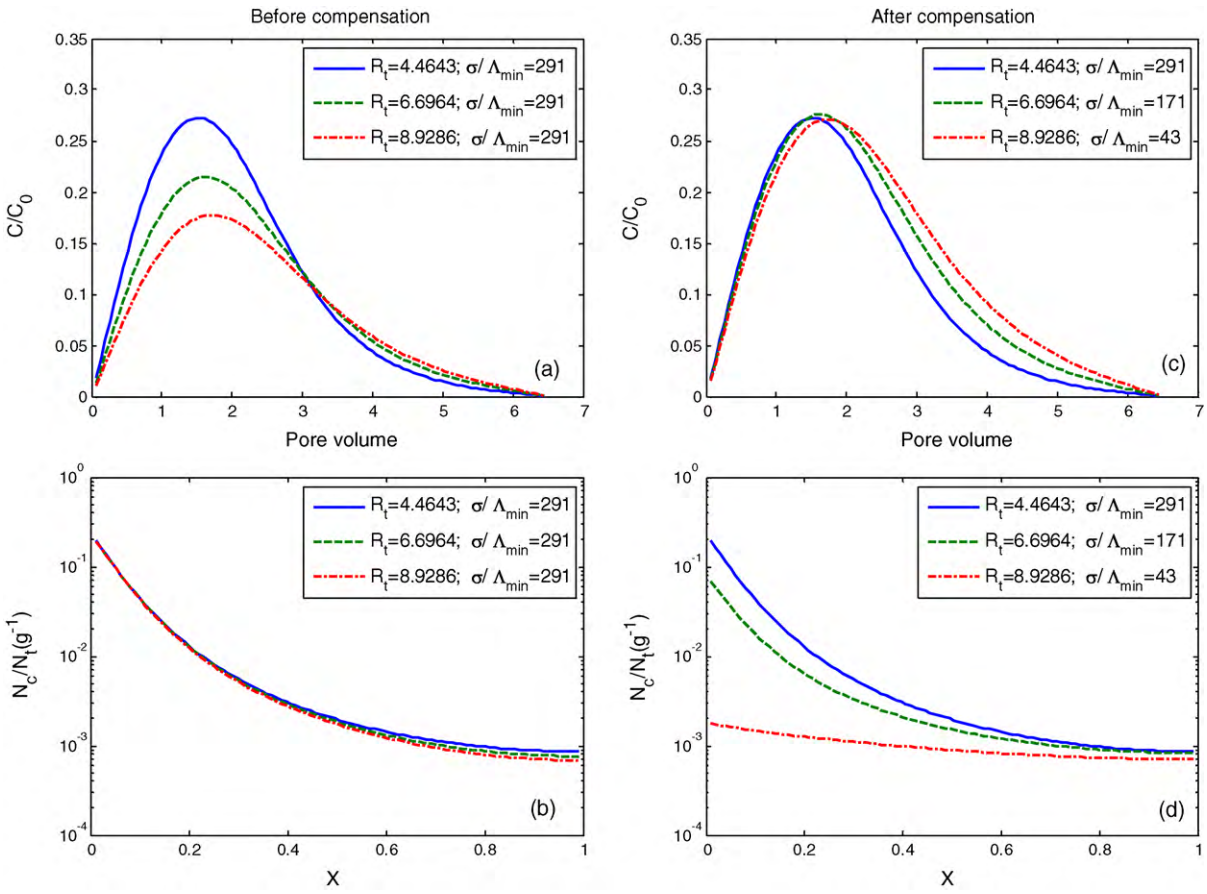

Fig. 6. Illustration of the temporal dispersion compensated for by the distribution of filtration coefficients. (a) and (b) Increase of the temporal dispersion and keeping the standard deviation of the distribution. (c) and (d) Increase of the temporal dispersion with decreasing standard deviations of the distribution.

4.1. Colloid in uniformly packed glass beads

In this subsection the results of numerical modeling are compared with the experiments carried out with artificial homogeneous porous media. Tufenkji and Elimelech [10] conducted column experiments on filtration of uniform polystyrene latex colloid suspension in packed soda-lime glass beads. The particles forming glass beads were of a uniform size and much larger than the colloid particles. A low influent concentration was adopted in order not to influence the pore structure. The solution chemistry was strictly controlled.

Calculations with the integral model are performed so as to reproduce the experimental results. The breakthrough curves predicted by the ADE and the experimental breakthrough curves highly agree with each other. Their shapes are almost not "washed-out" by dispersion. Therefore, it is reasonable to try modeling the experimental results by introducing the distribution of the filtration coefficients. Selection of the Λ distribution types for fitting the experiments follows a practical principle: few parameters to tune the shape of the distribution. Since the log-normal distribution cannot, apparently, provide significant deviations from the exponentiality of the deposition profiles observed in the experiments, it is not used for fitting. The bimodal distribution may seem to be physically reasonable for some cases [10], but there are as many as five parameters to be modified. The power law distribution with only three parameters to be modified is chosen due to its practical convenience in the computations. A similar choice was made in Ref. [15]. Because most of the power law distribution concentrates close to the minimum of the filtration coefficient, it is an important parameter as well as power b in Eq. (6).

Detailed parameters for the calculations are shown in Table 8. As seen in Fig. 7(b) and (d), after fitting the breakthrough curves, both the ADE with a single Λ and the elliptic equation with a single Λ predict (almost) exponential deposition profiles. The reason is the limitations on the variation of the temporal dispersion coefficient R_t caused by limited dispersion of the breakthrough curves. Meanwhile, the experimental results show that even for these monodisperse colloid suspensions the deposition profiles are hyperexponential. The results of the previous section indicate that the distribution of Λ may not be fully reflected by the shape of the breakthrough curves; therefore the properties of the distribution need to be fitted to the deposition profiles. The results show that

Table 8
Parameters adopted for calculations in comparison with the experiments of Tufenkji and Elimelech [10], corresponding to ionic strengths of 200 mM/100 mM respectively. Results are shown in Fig. 7.

Methodology	R_x ($\times 10^{-3}$)	R_t ($\times 10^{-3}$)	Λ_{min} ($\times 10^{-2}$)	Λ_{max} ($\times 10^{-2}$)	b
ADE + single Λ	4.17/4.17	0	47.20/8.74	47.20/8.74	–/–
ADE + distributed Λ	4.17/7.93	0	33.00/2.04	9102/955.71	1.90/1.50
Elliptic + single Λ	1.59/1.59	5.15	45.50/8.74	45.5/8.74	–/–
Elliptic + distributed Λ	1.59/1.59	3.43	34.97/2.04	9557.10/955.71	1.90/1.50

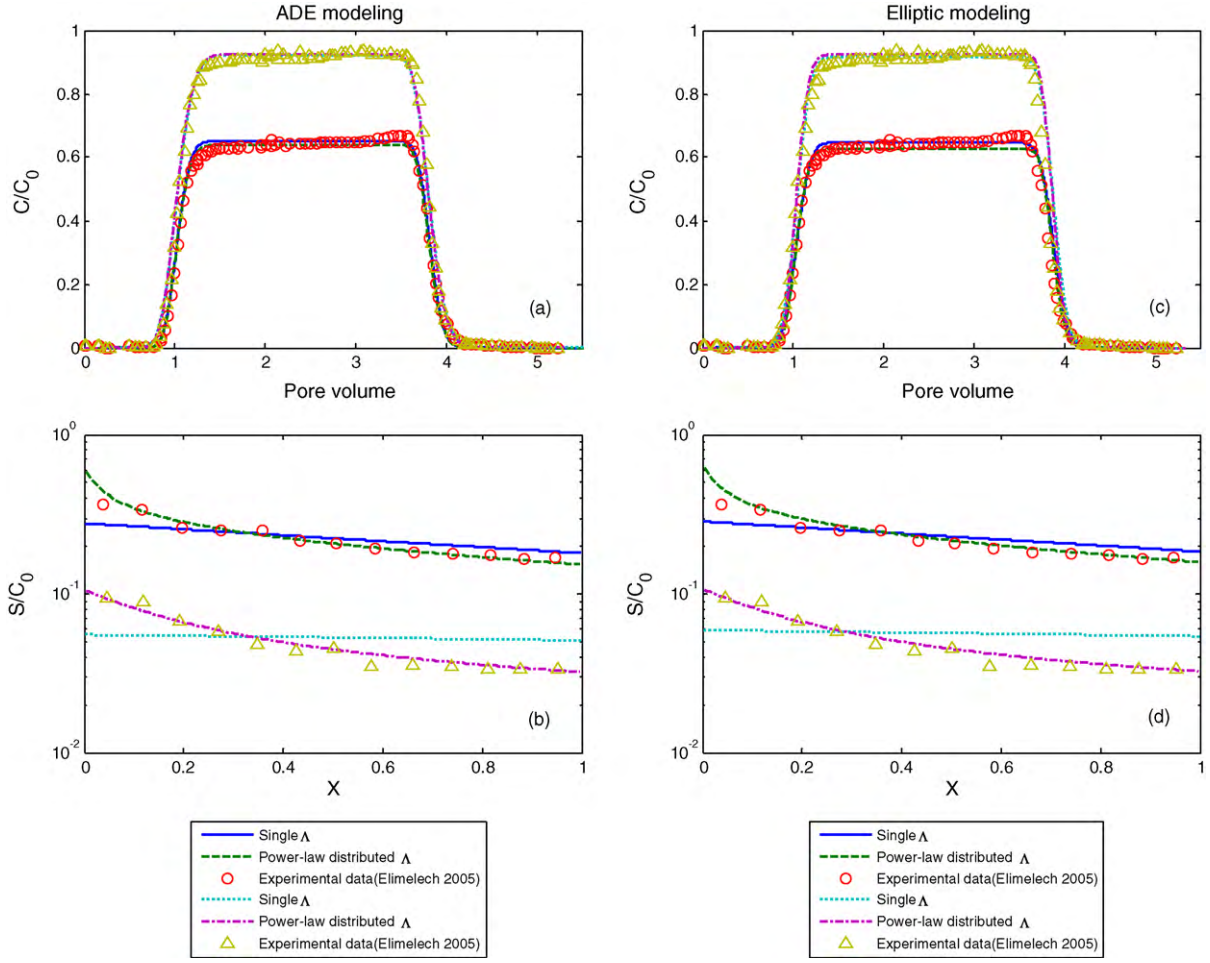

Fig. 7. Numerical modeling results compared with the experimental data of Tufenkji and Elimelech [10]. (a) and (b) ADE modeling; (c) and (d) elliptic modeling. The power law distribution is adopted.

the ADE with distributed filtration coefficients is sufficient to fit both the breakthrough curves and the hyperexponential deposition profiles. The fitted temporal dispersion in the elliptic equation is not large enough to yield a clearly hyperexponential deposition profile. Imposing a larger temporal dispersion would result in prohibitive modification of the breakthrough curve. The fact that the dispersion is not large is probably attributed to a high degree of homogeneity of the porous medium used for the experiment.

It should be remarked that the distribution of the filtration coefficients turns out to be rather wide, in spite of the apparent homogeneity of the particle population, as was also observed in Ref. [10]. The reason for the hyperexponentiality in this case is explained by the authors to be the presence of repulsive DLVO interactions. Under the unfavorable surface attachment conditions, the particles overcoming energy barriers to reach the primary energy minimum deposit slower, while others deposit faster. Such heterogeneity of interactions between the particles and the porous medium is the direct cause of the hyperexponential deposition profile. The same authors also managed to apply the ADE with a bimodal distribution of filtration coefficients to fit the experiments under similar conditions in Ref. [32].

4.2. Colloid in uniformly packed sand

The next experimental study considers suspension flow in a, apparently, more heterogeneous porous medium. Bradford et al. [19] adopted yellow–green fluorescent latex microspheres as colloid particles and packed Ottawa sand (99.8% quartz) as porous media for the column experiments. The sand particles were randomly shaped but uniformly sized and much larger than the colloid particles. As in the previous experiments, a low influent concentration was adopted in order not to influence the pore structure, and the solution chemistry was strictly controlled.

A number of calculations are carried out, trying to reproduce the results of Bradford et al. with the complete model involving the filtration coefficients distribution and the temporal dispersion. The common parameters in the calculations were $u = 1$, $\Lambda_{\max} = 1400$. The rest of the parameters are given in Table 9. As seen in Fig. 8, for

Table 9
Parameters adopted for modeling in comparison with experiments of Bradford et al. [19], in sequence: $d_c/d_{50} = 0.008/0.013/0.020$. Results are shown in Figs. 8 and 9.

Methodology	R_x ($\times 10^{-3}$)	R_t ($\times 10^{-3}$)	$\Lambda_{\min}$ ($\times 10^{-2}$)	$\Lambda_{\max}$ ($\times 10^{-2}$)	b
ADE + single Λ	6.98/4.07/0.78	0/0/0	0.42/1.70/2.52	0/0/0	–
ADE + distributed Λ	7.75/8.13/7.03	0/0/0	0.31/1.36/2.24	137.54/203.14/268.80	1
Elliptic + single Λ	4.98/4.07/0.78	1.80/4.40/7.10	0.42/1.70/2.52	0/0/0	–
Elliptic + distributed Λ	7.75/8.13/7.03	0.35/0.44/0.36	0.31/1.36/2.24	137.54/203.14/268.80	1

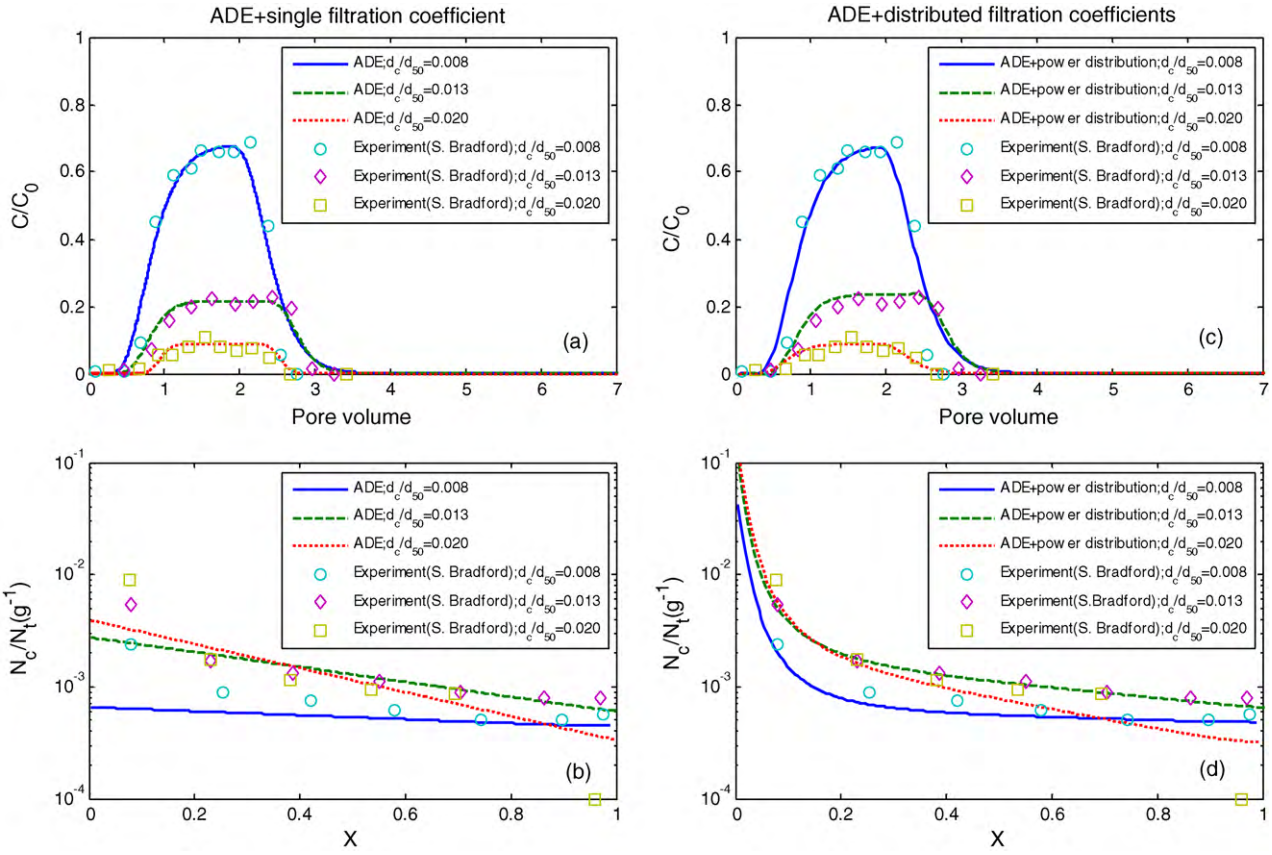

Fig. 8. ADE modeling results compared with S. Bradford's experimental data [19] with homogeneous porous media. The power law distribution is adopted.

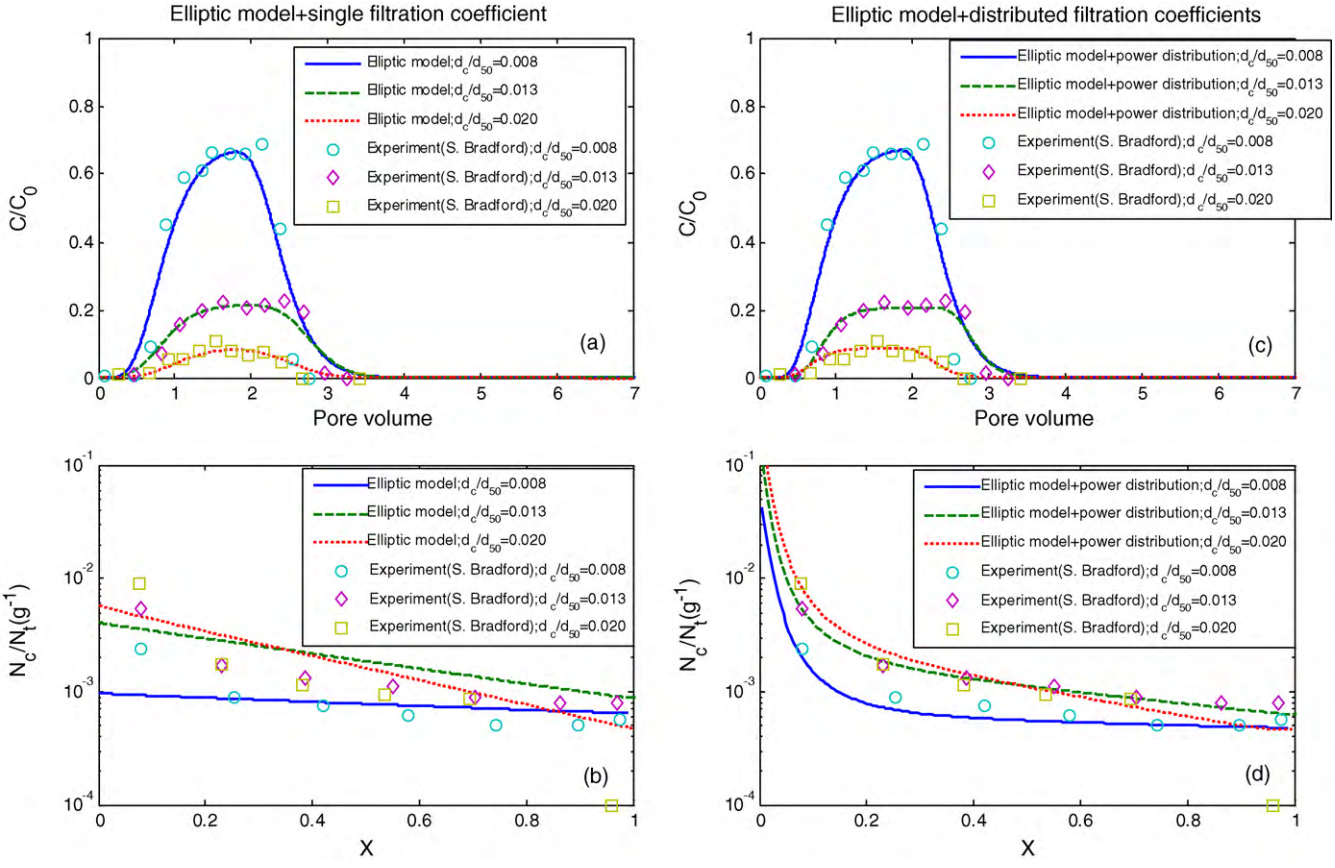

Fig. 9. Elliptic modeling results compared with Bradford's experimental data [19] with homogeneous porous media. The power law distribution is adopted.

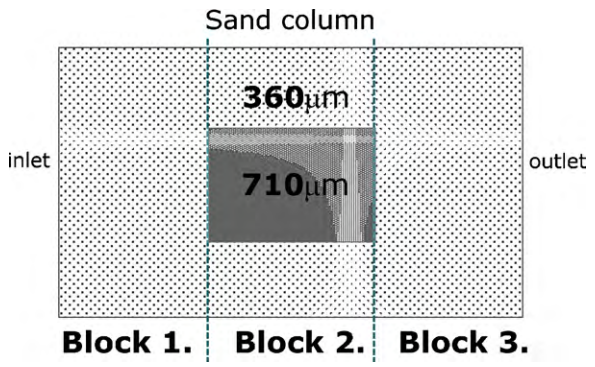

Fig. 10. Schematic illustration of the experiment conducted by Bradford et al. [25], the sand lens of 710 μm is in the center, and the sand matrix of 360 μm is outside.

these monodisperse colloid suspensions the experimental deposition profiles are hyperexponential. Although the breakthrough curves are more dispersed than in the previous set of the experiments, the dispersion is still relatively mild.

The distribution of Λ gives rise to hyperexponential deposition decay in compliance with the experimental observations. It should be noted, however, that the applied distribution is rather wide, which does not look fully realistic for a monodisperse suspension.

The experiment has also been simulated with a monodisperse suspension (a single value of Λ), but with a non-zero temporal dispersion. As seen in Fig. 9(a) and (c), the temporal dispersion fitted to match the observed breakthrough curves is still not large enough to predict clearly hyperexponential deposition profiles. The homogeneity of the porous media used in the experiments is likely to lead to Fickian transport with moderate temporal dispersion coefficients. The experimental results with homogeneous porous media can neither confirm the existence of nor the influence of temporal dispersion. On the contrary, the ADE with distributed filtration coefficients suffices to predict both the breakthrough curves and the deposition profiles. The best-fit parameters for the different ways of modeling are summarized in Table 9.

The DLVO calculations and the torque analysis by the authors of Ref. [19] show that the experimental conditions are also unfavorable for the surface attachment. The main mechanism of particle deposition is straining by design. Effects of straining are observed to be influenced by the grain sizes, grain shapes, hydrodynamics and solution chemistry. The heterogeneity of these factors is likely to cause the deposition hyperexponentiality. Compared to the experiment by Tufenkji and Elimelech [10], the authors adopted a more heterogeneous porous medium which gives rise to higher heterogeneity of particle-medium interactions. It may also explain why the degree of the deposition hyperexponentiality in this case is clearly higher. In Ref. [24], one of the same authors proposed a stochastic model for deep bed filtration also applying the distribution of filtration coefficients (log-normal and bimodal).

4.3. Colloid in non-uniformly packed sand

Since in relatively homogenous porous media temporal dispersion is not large enough to yield a hyperexponential deposition profile, comparison between the modeling and the experiments with highly heterogeneous porous media is of significance for the present study.

Bradford et al. [25] adopted carboxyl latex microspheres as colloid particles and Ottawa sand (99.8% quartz) as porous media for the column experiments. The heterogeneous system consisted of two types of soil, a soil cylinder lens (2.6 cm diameter, 6 cm long) embedded in the center of a second soil referred to as the matrix (5 cm diameter, 10 cm long), as shown in Fig. 10. Median particle

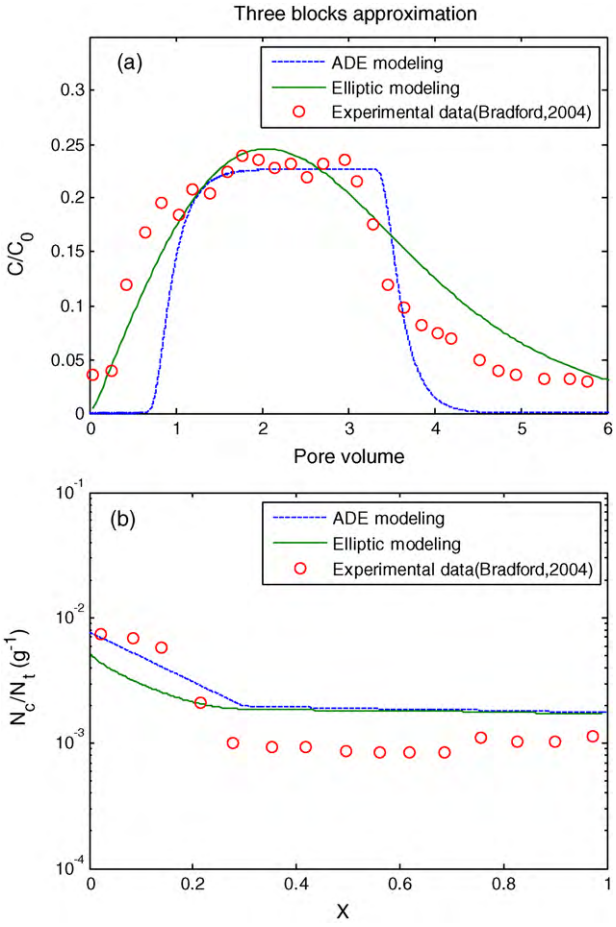

Fig. 11. Numerical modeling result compared with experimental observations, with the porous media approximated by three blocks in line.

sizes of the lens and the matrix were different. The chosen experiment adopted sand consisting of particles of 710 μm as the lens inside and sand of 360 μm as the matrix outside. A characteristic size of a colloid particle was 3.2 μm.

The deposition profile in this experiment is hyperexponential. Whether the hyperexponentiality is caused by temporal dispersion or by the spatial distribution of the filtration coefficients, is to be figured out.

In this experiment, the heterogeneity of the porous medium is known in advance, and it is essentially two-dimensional. Meanwhile, only a single-dimensional simulator has been prepared in this study. Therefore, two simplified representations of the porous column have been adopted. The first representation approximates the column as three blocks in line, as seen in Fig. 10. The side blocks are "pure", while the central block is "mixed". The second approach is, simply, to represent the column as a single block. In the latter regime, the effect of the heterogeneity is only encoded in the temporal dispersion term from the elliptic equation. The parameters for the calculations are shown in Table 10.

As seen in Fig. 11, both the ADE modeling and the elliptic modeling with the porous media approximated by three blocks are able to produce hyperexponential deposition profiles. Hyperexponentiality of the deposition is caused by spatial distribution of the filtration coefficients. Unlike the ADE, the elliptic equation can better describe the BTC, "catching" early arrival of the suspension and the large ending tail in the breakthrough curve. The deposition profile predicted by the ADE is composed of the three exponential decays. Transitions between them are abrupt (especially, between the first two cuts). The deposition profile predicted by the ellip-

Table 10
Parameters adopted for ADE/elliptic modeling in comparison with the experiments of Bradford et al. [25]. Results are shown in Figs. 11 and 12.

Upscaling regime	R_x	R_t	Λ
Three blocks			
Block 1	0.0033/1.00	0/22.27	1.33/0.85
Block 2	0.3333/13.33	0/0.05	0.61/0.57
Block 3	0.0033/13.33	0/22.27	0.61/0.85
Single block	0.10/4.00	0/25.03	1.80/2.94

tic equation also consists of the three parts, the first of which is smoother and is clearly hyperexponential. The transition between the first two phases is much smoother.

The second approach, where the porous medium is considered as a single block, is represented in Fig. 12. For this approach, the elliptic model is able to produce a hyperexponential deposition profile, while the ADE is not. Only the elliptic equation can catch the early arrival and the large ending tail on the breakthrough curve. The degree of hyperexponentiality caused by the temporal dispersion alone is not as high as the degree of hyperexponentiality observed in experiments or that obtained by the model of three blocks described above.

It can be deduced from the results above that, in this case, the deposition hyperexponentiality is caused both by the spatial distribution of the filtration coefficients and by the temporal dispersion. It has not been possible to match the experimental results for this case as precisely as for previous cases, probably due to roughness of the one-dimensional representation.

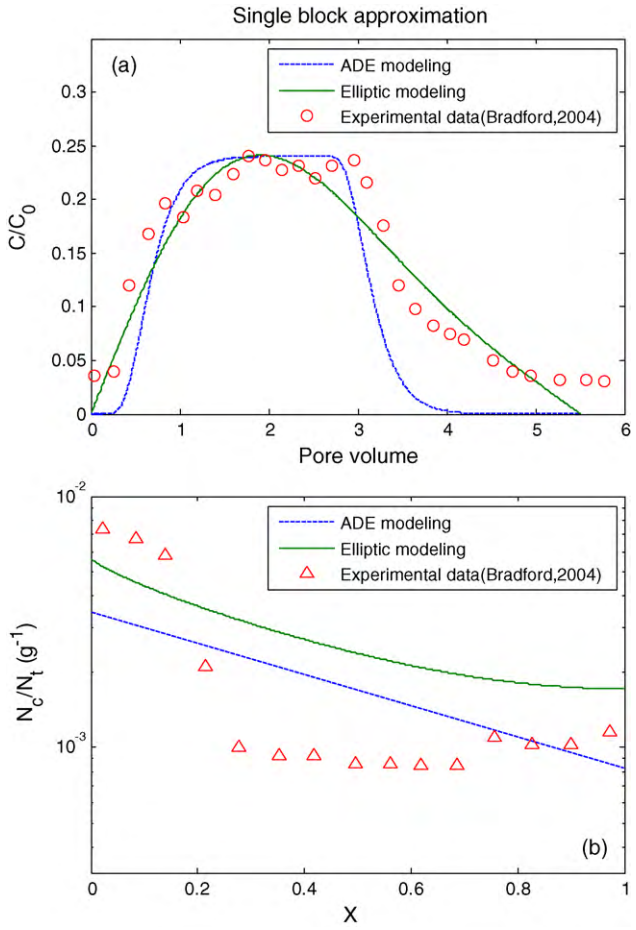

Fig. 12. Numerical modeling result compared with experimental observations, with the porous media approximated by a single block.

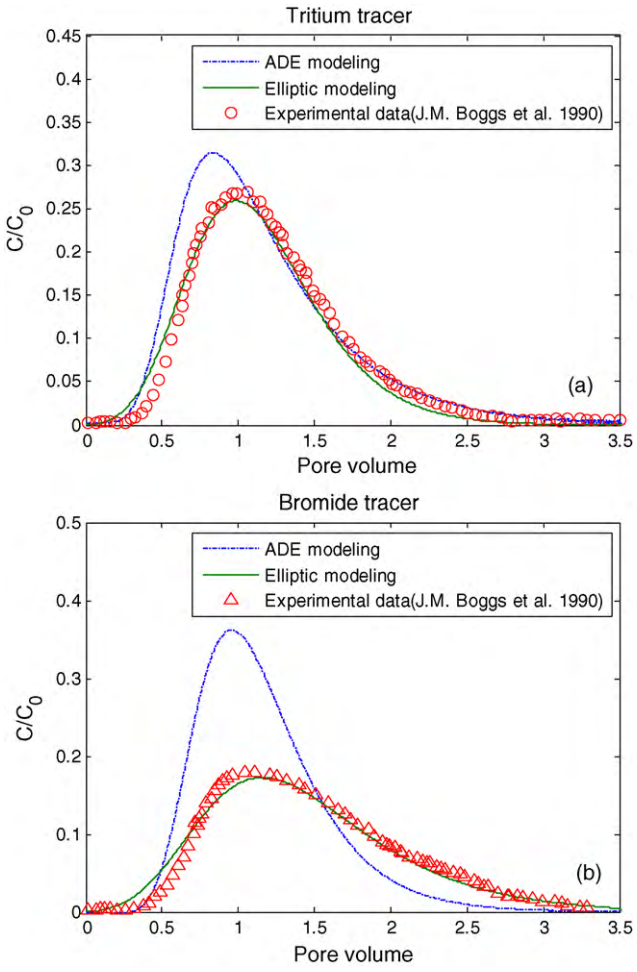

Fig. 13. Tracer injection in natural porous media. Numerical modeling results compared with the experimental observations by Boggs et al. [23].

4.4. Tracer injection in natural porous media

In order to confirm the ability of the elliptic equation to model non-Fickian transport in heterogeneous porous media, the modeling results are compared with tracer injection experiments. The physics of tracer injection is similar to that of the monodisperse suspension flow in porous media with a zero-filtration coefficient. The experiments described by Boggs et al. have been carried out with natural aquifer material from a field site located at Columbus Air Force base in northeastern Mississippi [23]. They adopted a column with a diameter of 5.2 cm and lengths of 100 cm. Tracers with tritium and calcium bromide were injected at a flow rate of 4.8 cm/day.

The breakthrough curves from the ADE and elliptic models are compared with the experimental observations, as seen in Fig. 13. The modeling parameters are summarized in Table 11. Compared to the result of the ADE, the experimental breakthrough curve is characterized by the delayed peak and the large ending tail. These are the two distinguishing features of non-Fickian transport in het-

Table 11
Parameters adopted for ADE/elliptic modeling in comparison with the experiments of Boggs et al. [23]. v is the tracer velocity, and v_{water} is the average pore water velocity. Results are shown in Fig. 13.

Tracer	R_x	R_t	v/v_{water}
Bromide	0.09/0.10	0/0.0518	0.90/0.73
Tritium	0.18/0.06	0/0.0544	0.80/1.00

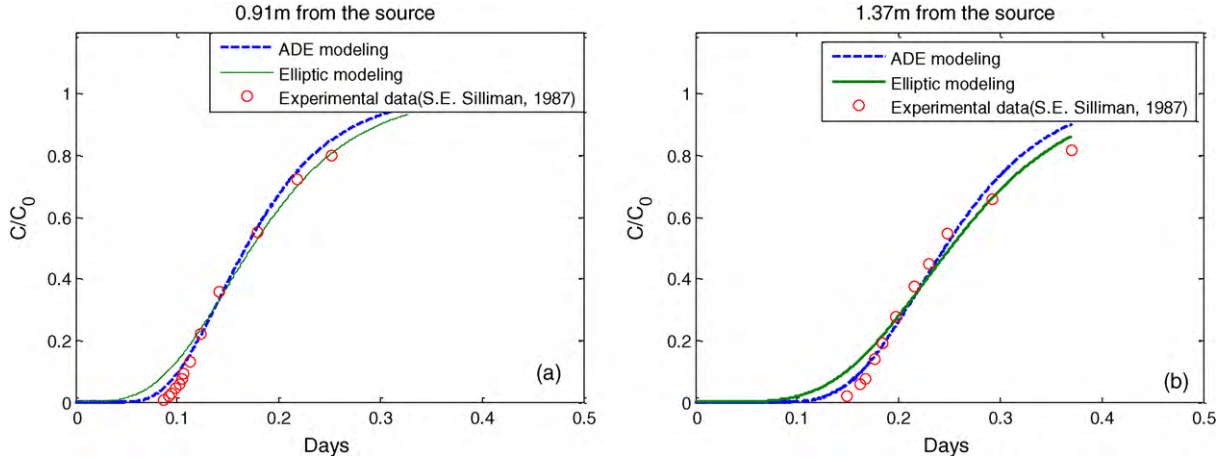

Fig. 14. Tracer injection in porous media with uniform heterogeneity. Numerical modeling results compared with the experimental observations by Silliman and Simpson [22].

erogeneous porous media. Unlike the ADE, the elliptic equation succeeds in modeling the highly asymmetric breakthrough curve. Nonetheless, the elliptic equation slightly overestimates the early arrival of the tracer around the breakthrough. In addition, the tracer velocity needs to be different from the average pore water velocity in order to fit the breakthrough curve successfully, as seen in Table 11.

It is also worth mentioning that, the parameters (velocity and dispersion coefficients) used for fitting the two breakthrough curves in the same porous medium are rather different in this case, while the parameters for fitting the experiments above and below are similar. It indicates that, for not-so-strongly heterogeneous porous media the parameters fitted to one experiment may be used for simulating another experiment, while for highly heterogeneous porous media they may not. It may be due to underestimating the really complicated physics in the natural porous media. Detailed study of this question is beyond the scope of the present work.

4.5. Tracer injection in porous media with uniform heterogeneity

Another experiment with heterogeneous media is carried out by Silliman and Simpson [22]. The experiment adopts an artificially heterogeneous porous medium with a coarse sand matrix and a number of small boxes of fine sand inside. The sand boxes are placed uniformly. The degree of heterogeneity is probably lower than in the experiments [23,25] modeled above.

The breakthrough curves from ADE modeling and elliptic modeling are compared with experimental observations, as seen in Fig. 14. The modeling parameters are presented in Table 12. ADE modeling is carried out with the best estimated parameters from Berkowitz and Scher [33]. Low temporal dispersion coefficients are adopted in the elliptic equation. Unlike the ADE, the elliptic equation can model the long "tails" of the integral breakthrough curves. However, it overestimates early arrival of the tracer.

Summarizing the comparisons between the modeling and the experiments, a method for estimating the parameters in the model may be described as follows. Ellipticity of the model may be ruled out in the first place if the effluent concentration profile is clearly stepwise. On the contrary, if this profile is smoothed, one may expect non-zero elliptic dispersion. The distribution of the filtration coefficients may be ruled out if the deposition is exponentially decreasing. For the case with a stepwise breakthrough curve and hyperexponential deposition, the ADE with distributed filtration coefficients is adequate. If ellipticity is nonzero, it may be sufficient to predict moderate hyperexponentiality without introducing distribution of filtration coefficients. The parameters for transport can be fitted to the breakthrough curve alone and the distribution of filtration coefficients (power law) can be fitted to the deposition profile alone. On the other hand, for the experiment with a widely dispersed breakthrough curve (early arrival, large tail) and hyperexponential deposition, the temporal dispersion coefficient needs to be fitted to the breakthrough curve first, and then the distribution is fitted to the deposition. After separate fitting of the dispersion coefficient and the distribution to match different curves, some "fine tuning" is required, to better match both curves. It is because the deposition hyperexponentiality may be attributed to both the temporal dispersion and the distribution of filtration coefficients.

Table 12
Parameters adopted for ADE/elliptic modeling in comparison with the experiments of Silliman and Simpson [22]. Results are shown in Fig. 14.

Position from source	R_x	R_t
0.91 m	0.0879/0.0879	0/0.0291
1.37 m	0.0547/0.0547	0/0.0212

5. Conclusions

The experimental data and our computations indicate that hyperexponentiality of the deposition can be caused by the following three mechanisms: particle population heterogeneity in connection with the distribution of the filtration coefficients, mid-scale heterogeneity in connection with non-Fickian transport, and macroscale heterogeneity in connection with spatial distribution of the filtration coefficients. The degree of "wash-out" of a breakthrough curve indicates whether the elliptic formalism is necessary. In cases where a breakthrough curve is (almost) stepwise (which is commonly observed for artificial uniform porous media), application of the elliptic formalism seems to be inadequate, and hyperexponentiality of the deposition profiles, if observed, should be caused by the explicit or implicit distribution of the parameters of the particles in the suspension. In non-uniform porous media the breakthrough curves may be more dispersed. For such cases the elliptic transport equation, probably, coupled with the particle distribution, seems to be more adequate.

The effects of the temporal dispersion and the distribution of filtration coefficients can be compensated for by each other, but not entirely. It implies that attributing the deposition hyperexponentiality to particle population heterogeneity alone or non-Fickian transport alone may be to overestimate this factor.

Acknowledgements

This work is funded by the Danish Council for Independent Research, Technology and Production Sciences (FTP), which is kindly acknowledged for financial support. Moreover, we would like to acknowledge Scott Bradford (the U.S. Agricultural Department) for providing the detailed experimental data.

References

[1] M. Elimelech, J. Gregory, R. Williams, X. Jia, Particle Deposition and Aggregation: Measurement, Modelling and Simulation (Colloid and Surface Engineering), Butterworth-Heinemann, 1998.
[2] F. Civan, Reservoir Formation Damage, Gulf Professional Publishing, USA, 2000.
[3] M. Fourar, G. Radilla, Non-Fickian description of tracer transport through heterogeneous porous media, Transport in Porous Media 80 (3) (2009) 561–579.
[4] A. Cortis, B. Berkowitz, Anomalous transport in "classical" soil and sand columns, Soil Science Society of America Journal 68 (5) (2004) 1539–1548.
[5] M. Levy, B. Berkowitz, Measurement and analysis of non-Fickian dispersion in heterogeneous porous media, Journal of Contaminant Hydrology 64 (3–4) (2003) 203–226.
[6] A.A. Shapiro, Elliptic equation for random walks. Application to transport in microporous media, Physica A: Statistical Mechanics and its Applications 375 (1) (2007) 81–96.
[7] A.A. Shapiro, P.G. Bedrikovetsky, Elliptic random-walk equation for suspension and tracer transport in porous media, Physica A: Statistical Mechanics and its Applications 387 (24) (2008) 5963–5978.
[8] A.A. Shapiro, P.G. Bedrikovetsky, A stochastic theory for deep bed filtration accounting for dispersion and size distributions, Physica A: Statistical Mechanics and its Applications 389 (13) (2010) 2473–2494.
[9] J.P. Herzig, D.M. Leclerc, P.L. Goff, Flow of suspensions through porous media-application to deep filtration, Industrial & Engineering Chemistry 62 (5) (1970) 8–35.
[10] N. Tufenkji, M. Elimelech, Breakdown of colloid filtration theory: role of the secondary energy minimum and surface charge heterogeneities, Langmuir 21 (3) (2005) 841–852.
[11] X. Li, W.P. Johnson, Nonmonotonic variations in deposition rate coefficients of microspheres in porous media under unfavorable deposition conditions, Environmental Science & Technology 39 (6) (2005) 1658–1665.
[12] X. Li, C.-L. Lin, J.D. Miller, W.P. Johnson, Role of grain-to-grain contacts on profiles of retained colloids in porous media in the presence of an energy barrier to deposition, Environmental Science & Technology 40 (12) (2006) 3769–3774.
[13] M. Tong, W.P. Johnson, Colloid population heterogeneity drives hyperexponential deviation from classic filtration theory, Environmental Science & Technology 41 (2) (2006) 493–499.
[14] N. Tufenkji, M. Elimelech, Reply to comment on breakdown of colloid filtration theory: role of the secondary energy minimum and surface charge heterogeneities, Langmuir 21 (23) (2005) 10896–10897.
[15] N. Tufenkji, J.A. Redman, M. Elimelech, Interpreting deposition patterns of microbial particles in laboratory-scale column experiments, Environmental Science & Technology 37 (3) (2003) 616–623.
[16] R.C. Bales, S.R. Hinkle, T.W. Kroeger, K. Stocking, C.P. Gerba, Bacteriophage adsorption during transport through porous media: chemical perturbations and reversibility, Environmental Science & Technology 25 (12) (1991) 2088–2095.
[17] J.A. Fitzpatrick, L.A. Spielman, Filtration of aqueous latex suspensions through beds of glass spheres, Journal of Colloid and Interface Science 43 (2) (1973) 350–369.
[18] K.A. Newman, K.D. Stolzenbach, Kinetics of aggregation and disaggregation of titanium dioxide particles and glass beads in a sheared fluid suspension, Colloids and Surfaces A: Physicochemical and Engineering Aspects 107 (1996) 189–203.
[19] S.A. Bradford, S. Torkzaban, S.L. Walker, Coupling of physical and chemical mechanisms of colloid straining in saturated porous media, Water Research 41 (13) (2007) 3012–3024.
[20] J.A. Redman, M.K. Estes, S.B. Grant, Resolving macroscale and microscale heterogeneity in virus filtration, Colloids and Surfaces A: Physicochemical and Engineering Aspects 191 (1–2) (2001) 57–70.
[21] J.A. Redman, S.B. Grant, T.M. Olson, M.K. Estes, Pathogen filtration, heterogeneity, and the potable reuse of wastewater, Environmental Science & Technology 35 (9) (2001) 1798–1805.
[22] S.E. Silliman, E.S. Simpson, Laboratory evidence of the scale effect in dispersion of solutes in porous media, Water Resources Research 23 (8) (1987) 1667–1673.
[23] J.M. Boggs, S.C. Young, W.R. Waldrop, L.W. Gelhar, E.E. Adams, K.R. Rehfeldt, Field study of macrodispersion in a heterogeneous aquifer. 1. Overview of tracer experiment AECL Report Series, 1990, pp. 34–56.
[24] S.A. Bradford, N. Toride, A stochastic model for colloid transport and deposition, Journal of Environmental Quality 36 (2007) 1346–1356.
[25] S.A. Bradford, M. Bettahar, J. Simunek, M.T.v. Genuchten, Straining and attachment of colloids in physically heterogeneous porous media, Vadose Zone Journal 3 (2004) 384–394.
[26] C.H. Bolster, A.L. Mills, G.M. Hornberger, J.S. Herman, Spatial distribution of deposited bacteria following miscible displacement experiments in intact cores, Water Resources Research 35 (6) (1999) 1797–1808.
[27] J.C. Baygents, J.R. Glynn, O. Albinger, B.K. Biesemeyer, K.L. Ogden, R.G. Arnold, Variation of surface charge density in monoclonal bacterial populations: implications for transport through porous media, Environmental Science & Technology 32 (11) (1998) 1596–1603.
[28] S.F. Simoni, H. Harms, T.N.P. Bosma, A.J.B. Zehnder, Population heterogeneity affects transport of bacteria through sand columns at low flow rates, Environmental Science & Technology 32 (14) (1998) 2100–2105.
[29] G.H. Golub, C.F.V. Loan, Matrix Computations (Johns Hopkins Studies in Mathematical Sciences), The Johns Hopkins University Press, USA, 1996.
[30] V. Shah, J. Gilbert, Sparse Matrices in Matlab *P: Design and Implementation, High Performance Computing – HiPC 2004, 2005, pp. 144–155.
[31] P.V. Danckwerts, Continuous flow systems. Distribution of residence times, Chemical Engineering Science 50 (24) (1995) 3857–3866.
[32] N. Tufenkji, M. Elimelech, Deviation from the classical colloid filtration theory in the presence of repulsive DLVO interactions, Langmuir 20 (25) (2004) 10818–10828.
[33] B. Berkowitz, H. Scher, The role of probabilistic approaches to transport theory in heterogeneous media, Transport in Porous Media 42 (1) (2001) 241–263.